Forward models for multimodal functional imaging

Maureen Clerc

Inria Sophia Antipolis

November 21, 2017

Outline

Introduction

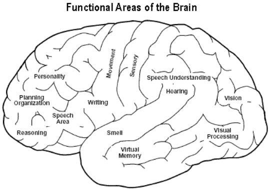

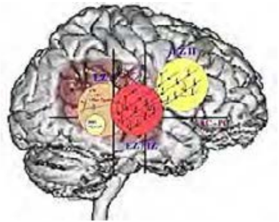

Functional areas of the brain

- schematic organization
- variability of cortical foldings
- subject-dependent localization through exploration

How to localize brain activity:

- invasively: brain stimulation
- non-invasively: functional brain imaging

Presurgical evaluation of epilepsy

- Epileptogenic regions
- Eloquent functional regions

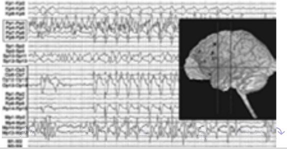

Introduction

1924: Hans Berger measures electrical potential variations on the scalp.

- birth of **Electro-Encephalography (EEG)**
- several types of oscillations detected (alpha 10 Hz, beta 15 Hz)
- origin of the signal unclear at the time
- scalp topographies ressembling dipolar field patterns

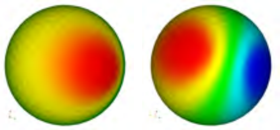

From electric to magnetic fields

A dipole generates both
an **electric** and a **magnetic** field

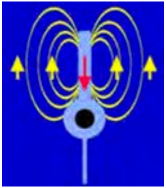

electric field lines

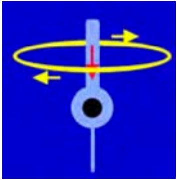

magnetic field lines

- 1963: Magnetocardiography,
- 1972: **Magneto-Encephalography (MEG)**, discovered by David Cohen, MIT,

  by measuring alpha waves, 40 years after EEG.
  Relies on a Superconductive QUantum Interference Device.

Advantage of MEG over EEG: spatially more focal

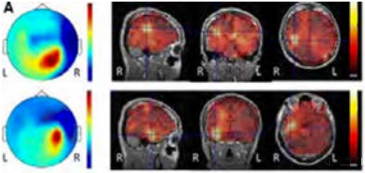

Strengths of magnetic fields

Very weak signal, measurable only in shielded environment

MR scanner	1	*(order of magnitude,*
	10^{-1}	*in Tesla)*
	10^{-2}	
	10^{-3}	
earth's field	10^{-4}	
	10^{-5}	
urban noise	10^{-6}	
	10^{-7}	
	10^{-8}	
car at 50m	10^{-9}	lung particles
screwdriver at 5m	10^{-10}	human heart
	10^{-11}	skeletal muscles, fetal heart
transistor at 2m	10^{-12}	human eye, **human brain (alpha)**
	10^{-13}	**human brain (evoked response)**
	10^{-14}	squid system noise level
	10^{-15}	

MEG instrumentation

MEG center, Institut Cerveau-Moëlle, Paris

MEG center, La Timone Hospital, Marseille

Origin of brain activity measured in EEG and MEG

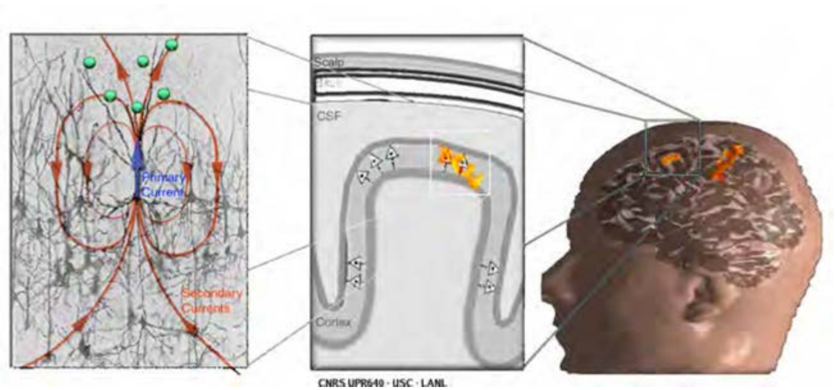

[Baillet et al., IEEE Signal Processing Mag, 2001]

Pyramidal neurons post-synaptic currents	Current perpendicular to cortical surface	Neurons in a macrocolumn co-activate

Bioelectricity follows quasistatic Maxwell

- origin of activity: depolarization / repolarization of neural membranes
- postsynaptic potentials represented by dipoles
- dipole positions located in grey matter
- dipole orientations perpendicular to cortical folds

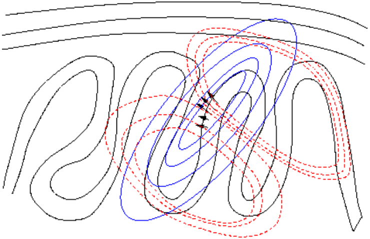

At low frequency (< 1000 Hz),
quasistatic approximation to Maxwell's equations:

- $\frac{\partial}{\partial t}$ negligible compared to $\frac{\partial}{\partial r}$
- electric field become decoupled from magnetic field (simpler than full Maxwell)

Electric field

Electric field $\vec{E}$ derives from an electric potential: $\vec{E} = -\nabla V$.
Ohmic current defined by $\sigma \vec{E} = -\sigma \nabla V$.
Total current = Ohmic current + primary current (brain activity):

$$\mathbf{J}_{\mathrm{tot}} = -\sigma \nabla V + \mathbf{J}^{\mathrm{p}}$$

Conservation of charge: $\nabla \cdot \mathbf{J}_{\mathrm{tot}} = 0$ thus

$$\nabla \cdot (-\sigma \nabla V + \mathbf{J}^{\mathrm{p}}) = 0$$

hence the electrostatic equation:

$$\nabla \cdot (\sigma \nabla V) = \nabla \cdot \mathbf{J}^{\mathrm{p}}$$

Linear relation between sources $\mathbf{J}^{\mathrm{p}}$ and electric potential V

Magnetic field

In quasistatic regime, Maxwell-Ampère equation becomes

$$\begin{aligned} \nabla \times \vec{\mathbf{B}} &= \mu_0 \mathbf{J}_{\mathrm{tot}} \\ &= \mu_0 \left(\mathbf{J}^{\mathsf{p}} - \sigma \nabla V \right) \end{aligned}$$

$\rightarrow$ Biot-Savart:

$$\begin{aligned} \mathbf{B}(\mathbf{r}) &= \frac{\mu_0}{4\pi} \int (\mathbf{J}^{\mathsf{p}}(\mathbf{r}') - \sigma \nabla V(\mathbf{r}')) \times \frac{\mathbf{r}-\mathbf{r}'}{\|\mathbf{r}-\mathbf{r}'\|^3} d\mathbf{r}' \\ &= \mathbf{B}_\infty(\mathbf{r}) - \frac{\mu_0}{4\pi} \int \sigma \nabla V(\mathbf{r}') \times \frac{\mathbf{r}-\mathbf{r}'}{\|\mathbf{r}-\mathbf{r}'\|^3} d\mathbf{r}' \end{aligned}$$

Contribution $\mathbf{B}_\infty(\mathbf{r})$ is “primary magnetic field” coming directly from the sources

Linear relation between sources $\mathbf{J}^{\mathsf{p}}$ and magnetic field $\mathbf{B}$

Outline

Volume conduction

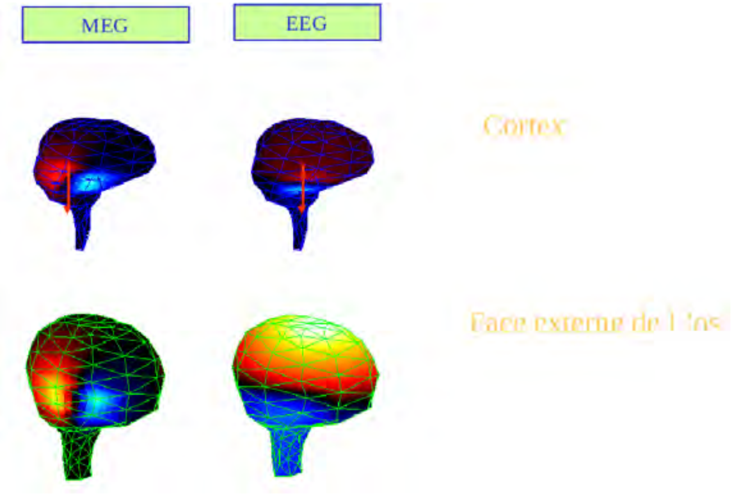

[courtesy of S.Baillet]

Influence of orientation (spherical geometry)

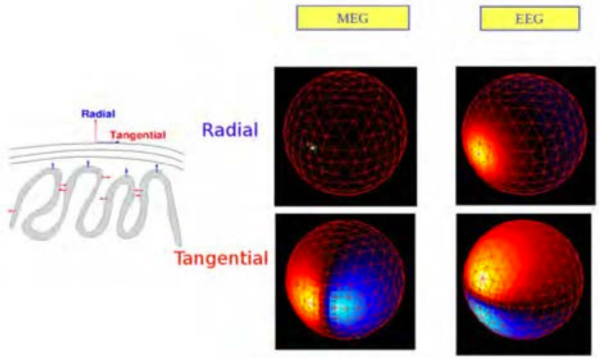

[courtesy of S.Baillet]

Influence of orientation (realistic geometry)

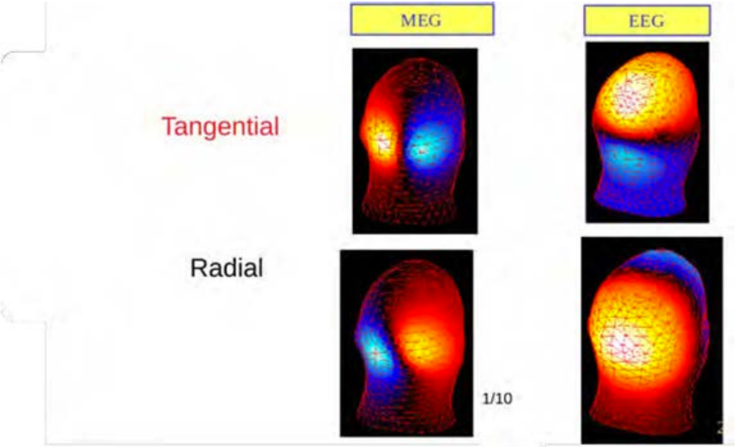

[courtesy of S.Baillet]

Influence of depth

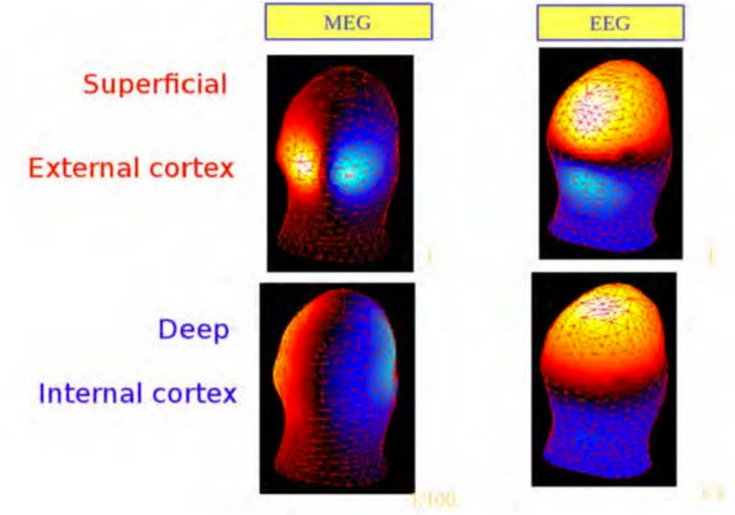

[courtesy of S.Baillet]

Consequences of volume conduction

Volume conduction produces a blurring effect

- depends on the modality (EEG, MEG, ECoG)
- EEG most diffuse (skull barrier)
- MEG more "transparent" to the skull
- ECoG under the skull, much less blurring.

Note: the spatial mixture is a curse, but also a blessing !

- EEG sensors sensitive to large areas of the cortex

Conversely, intracerebral electrodes only sensitive to close-by regions.

Consequences of volume conduction

A good understanding of the spatial mixture (forward problem) provides a key to unmixing the data (inverse problem):

Consequences of volume conduction

A good understanding of the spatial mixture (forward problem) provides a key to unmixing the data (inverse problem):

Consequences of volume conduction

The spatial mixture is instantaneous

- electromagnetic waves propagate at speed of light
- no "echo effect", nor delay, at the frequencies of interest for EEG

Nevertheless the spatial mixture also leads to a temporal mixture of signals

- effect on latencies
- effect on the frequency spectrum

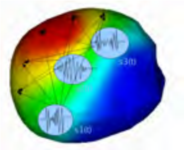

Volume conduction: consequences on time signals

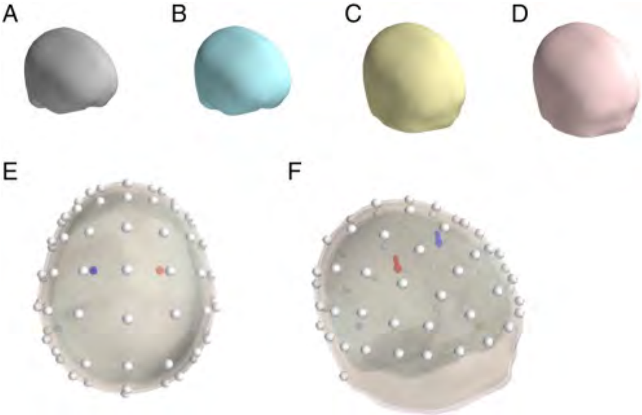

Right dipole (under C2): amplitude peak 100 ms
Left dipole (under C1): amplitude peak 250 ms
[Burle, Spieser et al, int J Psychophysiol. 2015]

Volume conduction: consequences on time signals

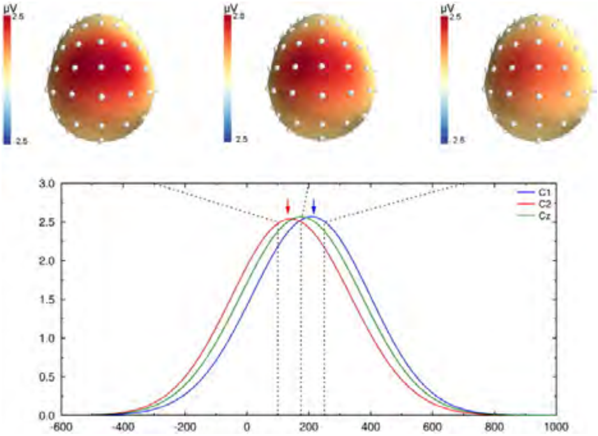

Volume conduction has an effect on time signals
→ **model it** in order to compensate for it

Conductivity σ

Relation between sources $\mathbf{J}^p$ and potential V

$$\nabla \cdot \sigma \nabla V = \nabla \cdot \mathbf{J}^p$$

- **Scalp, CSF, and gray matter:** σ isotropic ,
- **White matter:** σ anisotropic, depends on direction of fibers,
- **Skull:** σ inhomogeneous, anisotropic, holes.

EEG sensitive to $\sigma_{\text{scalp}}/\sigma_{\text{skull}}$ ratio [Vallaghé, Clerc IEEE TBME 2009]

	$\sigma_{\text{scalp}}/\sigma_{\text{skull}}$
Rush & Driscoll [1968]	80
Cohen & Cuffin [1983]	80
Oostendorp & al. [2000]	15
Gonçalves, de Munck etal. [2003]	$20 - 50$

Challenge: calibrating σ, non-invasively, in vivo:

- injecting known current on the scalp;
- multimodal measurements (MEG,EEG).

Influence of conductivity on localization

$\sigma_{\text{scalp}}/\sigma_{\text{skull}} = 80$ $\sigma_{\text{scalp}}/\sigma_{\text{skull}} = 40$ $\sigma_{\text{scalp}}/\sigma_{\text{skull}} = 20$

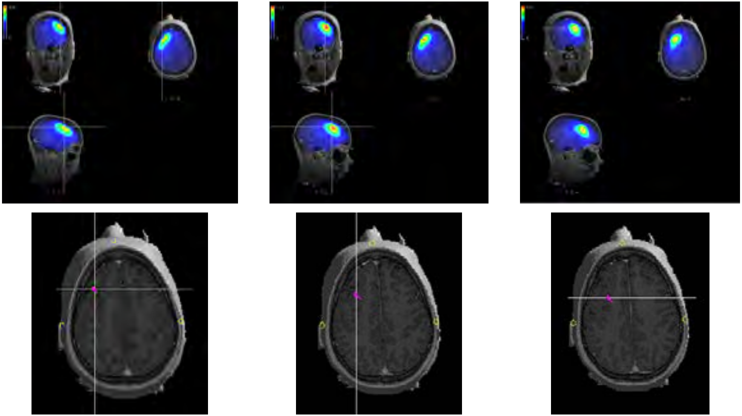

Averaged interictal spike.
Inverse reconstruction using MUSIC.

[courtesy of J-M Badier, La Timone]

Accounting for conductivity in M/EEG leadfields

- Skull conductivity: non homogeneous, compacta & spongiosa bone
- Conductivity estimation: uniqueness and robustness, influence of spongiosa on source localisation
- Fast Leadfields: Reduced bases to compute fast LF for a whole domain of conductivities. Mathematical guarantees on the approximation. Both source & conductivity estimation.

Influence of spongiosa | Leadfield as a function of conductivity | Approximation error

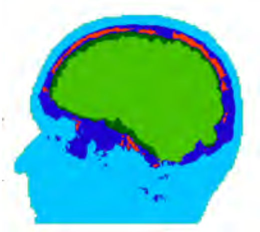

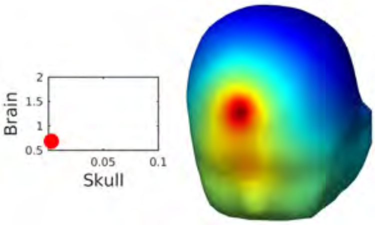

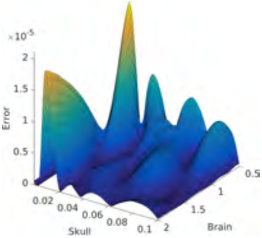

[Papageorgakis et al 2015] [Maksymenko et al 2017]

Outline

Model adaptation

- Individual variations:
  - Cortical foldings
  - Tissue conductivity
  - Tissue geometries
- Variations across sessions:
  - sensor positions

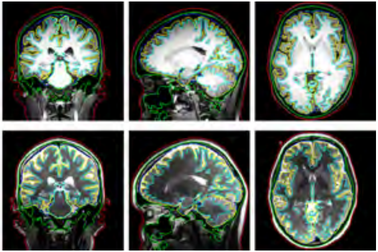

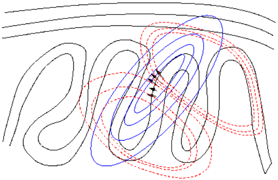

Take specificities into account in the *forward* problem to better solve the *inverse* source estimation problem

Fundamental "gain matrix"

Measurements **M** resulting from two sources:

- source $s_1(t)$ at position $\mathbf{x}_1$, orientation $\vec{q}_1$
- source $s_2(t)$ at position $\mathbf{x}_2$, orientation $\vec{q}_2$

$$\mathbf{M}(t) = \begin{bmatrix} G_1(x_1, \vec{q}_1) \\ \vdots \\ G_m(x_1, \vec{q}_1) \end{bmatrix} \times s_1(t) + \begin{bmatrix} G_1(x_2, \vec{q}_2) \\ \vdots \\ G_m(x_2, \vec{q}_2) \end{bmatrix} \times s_2(t)$$

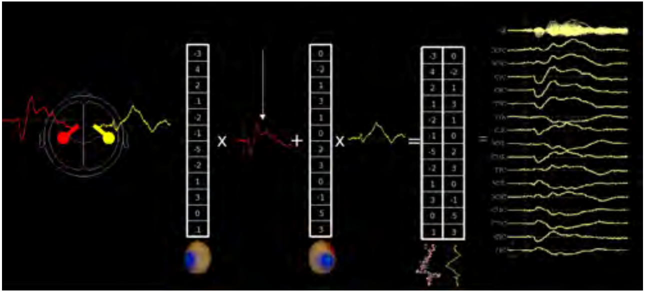

source: S. Baillet, Master MVA

From forward to inverse problem: the gain matrix

For n time samples $t_1 \ldots t_n$,

$$\mathbf{M} = \mathbf{G}\,\mathbf{S}$$

where **S** contains the source amplitudes

$$\mathbf{S} = \begin{bmatrix} s_1(t_1) & \ldots & s_1(t_n) \\ \vdots & \ddots & \vdots \\ s_N(t_1) & \ldots & s_N(t_n) \end{bmatrix}$$

Gain matrix

Gain matrix **G** computed via the Forward Problem,
provides **a linear relationship** between source amplitudes and sensor data.

Forward Problem

Given (cortical) source / (scalp) current distribution, compute electric potential, / magnetic field.

Quasistatic Maxwell links electric potential V to primary sources $\mathbf{J}^{\mathrm{p}}$:

$$\nabla \cdot (\sigma \nabla V) = \nabla \cdot \mathbf{J}^{\mathrm{p}} \ ,$$

current normal to the exterior surface:

$$\sigma \partial_{\mathbf{n}} V = j \ .^{1}$$

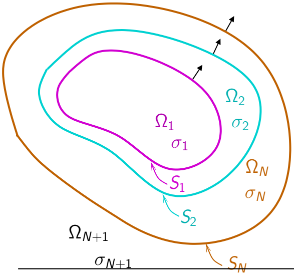

- Conductivity model: σ constant per domain.
- Potential V and normal current $\sigma \partial_{\mathbf{n}} V$ are continuous across interfaces S_i.
- Boundary integral theory: unknowns defined on interfaces.

[1] $\mathbf{n}$ normal vector, pointing outward.

Symmetric BEM matrix structure

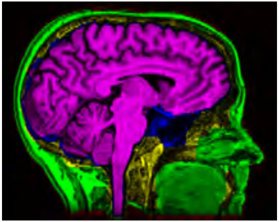

$$
\begin{bmatrix}
(\sigma_1+\sigma_2)N_{11} & -2D^*_{11} & -\sigma_2 N_{12} & D^*_{12} & & & \\
-2D_{11} & (\sigma_1^{-1}+\sigma_2^{-1})S_{11} & D_{12} & -\sigma_2^{-1}S_{12} & & & \\
-\sigma_2 N_{21} & D^*_{21} & (\sigma_2+\sigma_3)N_{22} & -2D^*_{22} & -\sigma_3 N_{23} & D^*_{23} & \\
D_{21} & -\sigma_2^{-1}S_{21} & -2D_{22} & (\sigma_2^{-1}+\sigma_3^{-1})S_{22} & D_{23} & -\sigma_3^{-1}S_{23} & \\
 & & -\sigma_3 N_{32} & D^*_{32} & (\sigma_3+\sigma_4)N_{33} & -2D^*_{33} & \cdots \\
 & & D_{32} & -\sigma_3^{-1}S_{32} & -2D_{33} & (\sigma_3^{-1}+\sigma_4^{-1})S_{33} & \cdots \\
 & & & & \vdots & \vdots & \ddots
\end{bmatrix}
\cdot
\begin{bmatrix} \mathbf{v}_1 \\ \mathbf{p}_1 \\ \mathbf{v}_2 \\ \mathbf{p}_2 \\ \mathbf{v}_3 \\ \mathbf{p}_3 \\ \vdots \end{bmatrix}
=
\begin{bmatrix} \sigma_1^{-1}N_{1\,sources} \\ D_{1\,sources} \\ 0 \\ 0 \\ 0 \\ 0 \\ \vdots \end{bmatrix}
.\mathbf{s}
$$

nH

nv1 nf1 nv2 nf2 nv3 nf3 nvS

[Kybic, Clerc et al, 2005]

Numerical validation of EEG accuracy

$$RDM = \left\| \frac{V}{\|V\|} - \frac{V_{an}}{\|V_{an}\|} \right\|$$

$$MAG = \left\| \frac{V}{V_{an}} \right\|$$

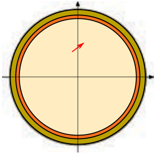

EEG
(regular meshes)

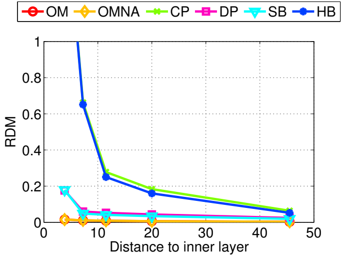

RDM 642 points/interface

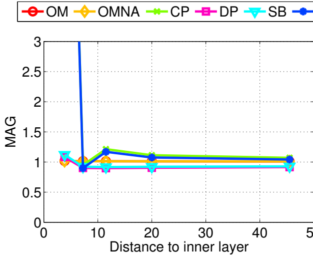

MAG 642 points/interface

BEM solvers tested:

OM	OMNA	CP	DP	SB	HB
OpenMEEG	OM non adaptive	Fieldtrip / CP	Fieldtrip / Dipoli	Simbio	Helsinki BEM

Opensource software: OpenMEEG

http://openmeeg.github.io [Gramfort, Papadopoulo, Olivi, Clerc, 2010]

- EEG and MEG
- Electrical stimulation (cochlear implants, tDCS)
- ElectroCorticography, stereo-encephalography

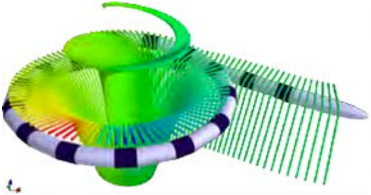

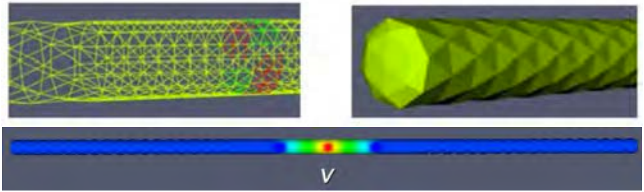

Skull defects

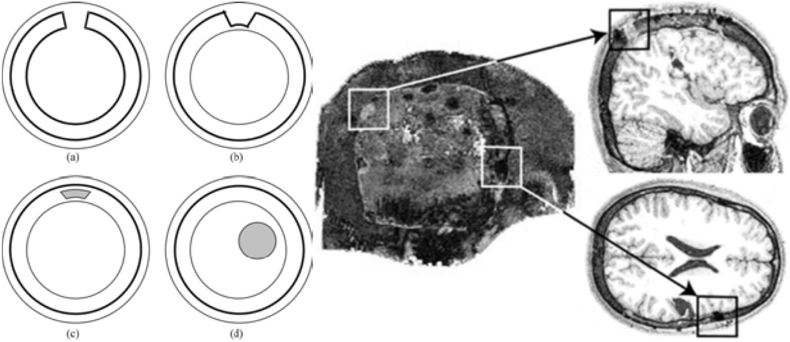

[Benar, Gotman 2001]

Beyond nested models

Boundary Element methods require piecewise-constant conductivity, not necessarily nested regions

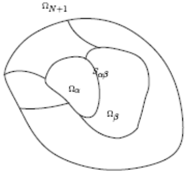

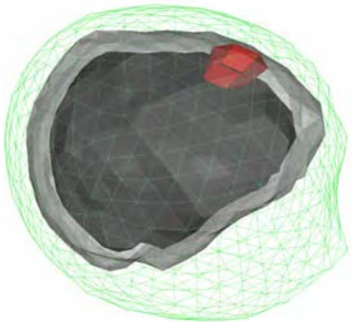

Symmetric BEM accommodates non-nested regions [Kybic et al 2006]
In latest OpenMEEG release.

Burr-hole model

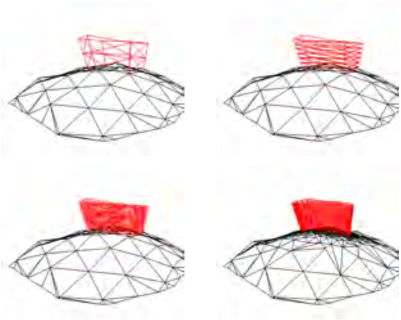

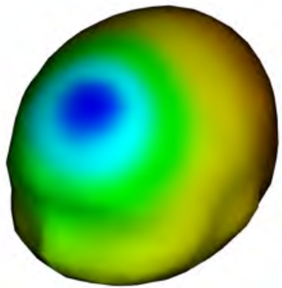

Mesh refinement necessary in the vicinity of sharp angles.

Skull defect

- 4-layer realistic (brain, CSF, skull, scalp)
- Burr hole due to surgery.

Goal: model burr-hole without meshing its surface

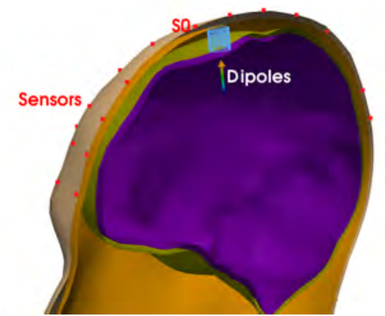

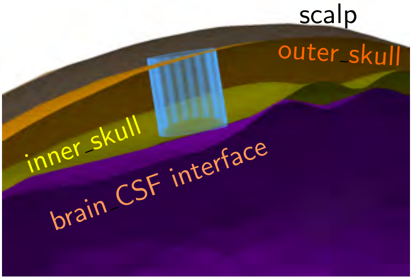

[Olivi 2011]

Skull defect

$$\begin{aligned} \nabla \cdot (\sigma \nabla V) &= 0 \quad \text{in Skull} \\ \sigma \Delta V + \nabla \cdot (\chi_h(\mathbf{r})(\sigma_h - \sigma)\nabla V) &= 0 \end{aligned}$$

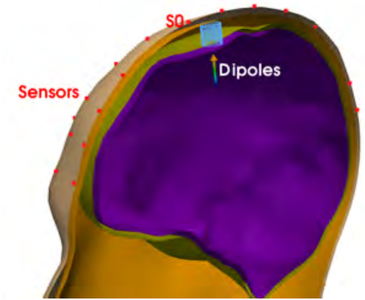

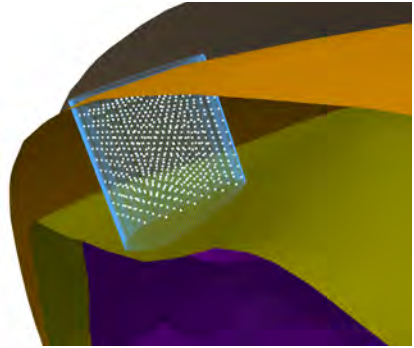

Skull defect

$$\begin{aligned} \nabla \cdot (\sigma \nabla V) &= 0 \quad \text{in Skull} \\ \sigma \Delta V + \nabla \cdot (\chi_h(\mathbf{r})(\sigma_h - \sigma)\nabla V) &= 0 \end{aligned}$$

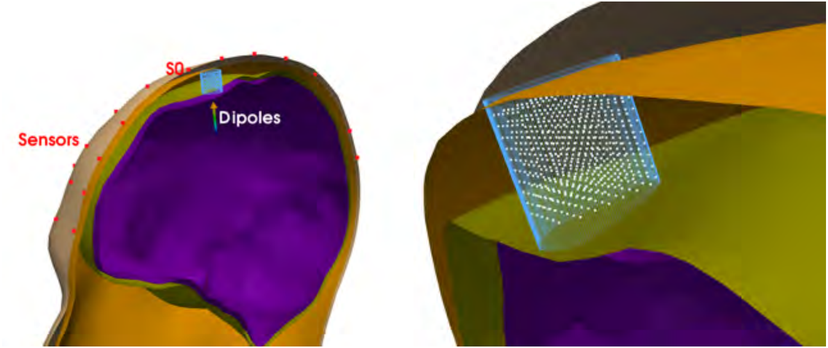

$$\sigma \Delta V^{k+1} = -\nabla \cdot \left(\sum_{i=1}^{N} (\mathbf{J}_i^x + \mathbf{J}_i^y + \mathbf{J}_i^z) \right) \text{ in Skull}$$

where $\mathbf{J}_i^x \sim (\sigma_h - \sigma)\mathbf{n}_x \nabla V(\mathbf{r}_i) \cdot \mathbf{n}_x \delta(\mathbf{r} - \mathbf{r}_i)$

Skull defect

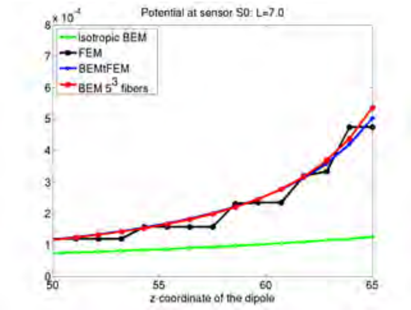

[Olivi et al 2011]

- simulate potential on sensor close to burr hole
- using 3*125 "virtual" dipoles
- perturbated model matches FEM

Outline

Source models: distributed or isolated

Distributed current source
defined on a surface S
with current density $q(\mathbf{r})$:

$$\mathbf{J}^{\mathrm{p}}(\mathbf{r}) = q(\mathbf{r})\,\mathbf{n}(\mathbf{r})\,\delta_S$$

($\mathbf{n}(\mathbf{r})$ orthogonal to S)

Isolated current dipole
defined at a position $\mathbf{p}$
with current (moment) $\mathbf{q}$:

$$\mathbf{J}^{\mathrm{p}} = \mathbf{q}\,\delta_{\mathbf{p}}$$

Also linear combinations

$$\mathbf{J}^{\mathrm{p}} = \sum_{i=1}^{n} \mathbf{q}_i\,\delta_{\mathbf{p}_i}$$

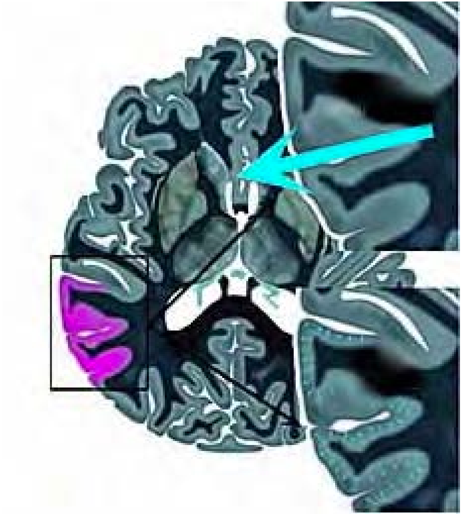

Source reconstruction

Two types of source models considered:

isolated	distributed
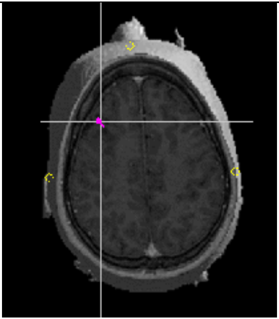	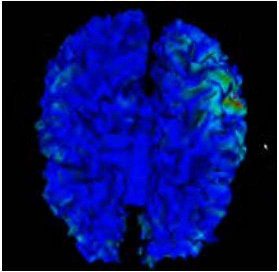
unknowns $\ll$ measurements sensitivity to model order	unknowns $\gg$ measurements indeterminacy regularization necessary

Uniqueness of reconstruction: proven for each model.
Ill-posedness, due to instability.

Source reconstruction: estimate **S** from **M**

Measurements on m EEG and/or MEG sensors.
The forward problem of volume conduction provides **G**:
a linear relationship between sources and sensor data:

$$\underbrace{\begin{bmatrix} M_1(t) \\ \vdots \\ M_m(t) \end{bmatrix}}_{\substack{m \times n \\ \mathbf{M}}} = \underbrace{\begin{bmatrix} G_1(x_1, \vec{q}_1) & \dots & G_1(x_p, \vec{q}_p) \\ \vdots & \ddots & \vdots \\ G_m(x_1, \vec{q}_1) & \dots & G_m(x_p, \vec{q}_p) \end{bmatrix}}_{\substack{m \times p \\ \mathbf{G} \text{ gain matrix}}} \underbrace{\begin{bmatrix} s_1(t) \\ \vdots \\ s_p(t) \end{bmatrix}}_{\substack{p \times n \\ \mathbf{S}}} + \mathbf{N}$$

$$\mathbf{M} = \mathbf{G}\,\mathbf{S} + \mathbf{N}$$

p sources $\gg$ m sensors

Regularized source reconstruction

Find sources **S** minimizing $\|\mathbf{M} - \mathbf{G}\,\mathbf{S}\|^2 + \lambda R(\mathbf{S})$
with $R(\mathbf{S})$: regularization.

Regularized Source Reconstruction

Finding **S** that minimizes

$$C(\mathbf{S}) = \|\mathbf{M} - \mathbf{G}\,\mathbf{S}\|^2 + \lambda R(\mathbf{S})$$

Many options for regularization $R(\mathbf{S})$.

L^2 regularization:

$$R(\mathbf{S}) = Tr(\mathbf{S}^T\mathbf{S})$$

Minimum Norm solution **S**

$$\mathbf{S} = \mathbf{G}^T(\mathbf{G}\mathbf{G}^T + \lambda\mathbf{I})^{-1}\mathbf{M}$$

Can be seen as a spatial filter applied to the measurements.

[Adde Clerc Keriven 2005]

Choice of λ see e.g. [Hincapié, Kujala, Mattout et al 2016]

Influence of regularization

simulated MEG, no noise

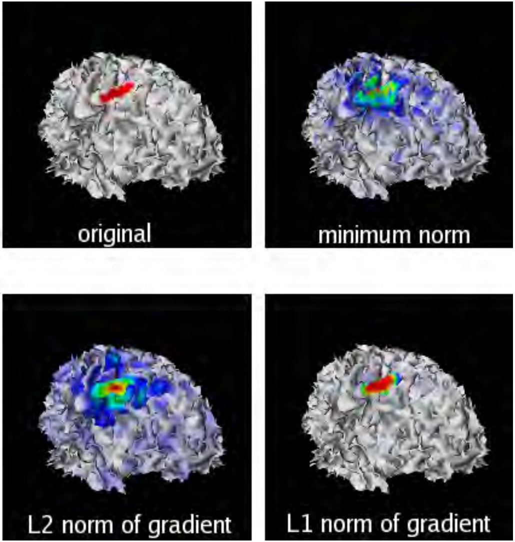

Influence of regularization

simulated MEG, 10% noise

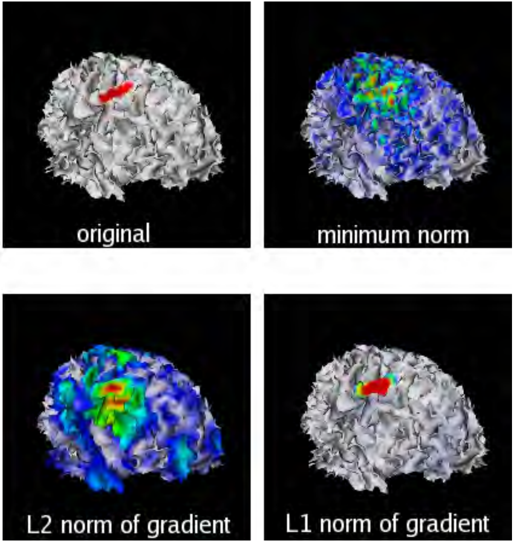

Influence of regularization

simulated EEG,
10% noise

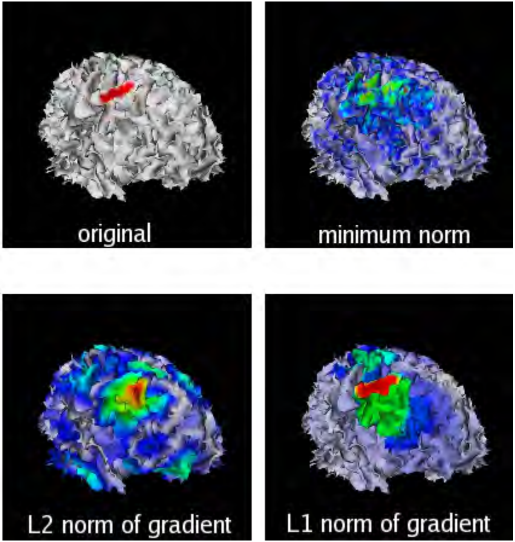

Outline

Tractography-based parcellation

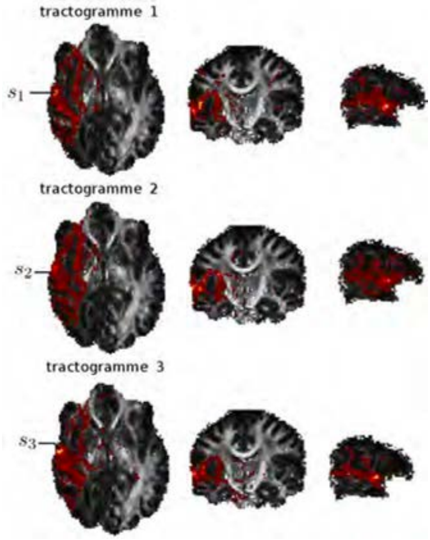

[Philippe et al 2017]

[Anwander 2007]
Correlation clustering of *CP*s:
Sources *i* and *j* clustered together if CP_i and CP_j similarly correlated to the *CP*s of all sources.
→ parcels

Anatomically constrained regularization

Find source distribution S such that

$$S = \text{argmin}_S \|M - GS\|^2 + \lambda \|S\|^2 + \mu \|W_P S\|_2^2$$

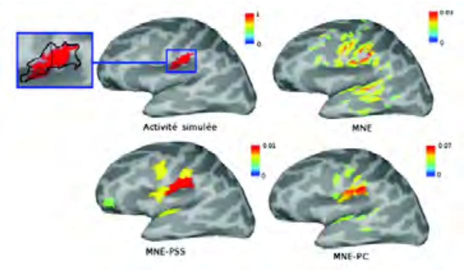

Comparison between:

- MNE $\mu = 0$
- MNE-PC W_P = parcellation-constrained Laplacian
- MNE-PSS MNE in reduced-dimensional source space (one scalar per parcel)

Epileptic spike propagation

- 1st step: clustering of spikes in time-domain (Inserm La Timone) $\rightarrow$ several classes
- 2nd step: source reconstruction for each class

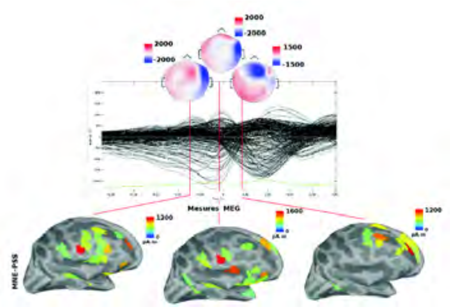

average spike

Epileptic spike propagation

- 1st step: clustering of spikes in time-domain (Inserm La Timone) $\rightarrow$ several classes
- 2nd step: source reconstruction for each class

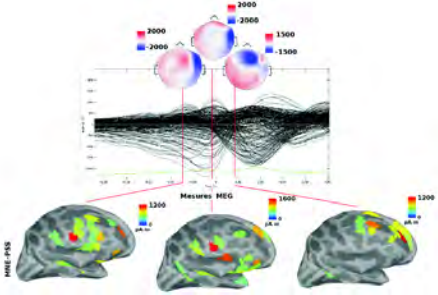

average spike

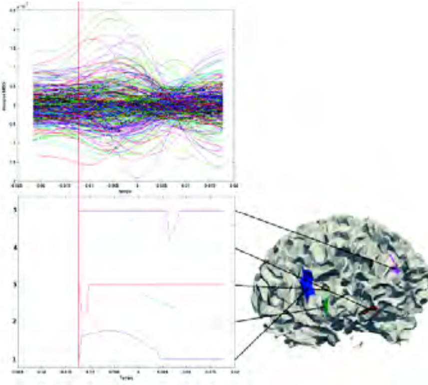

single spike

Similarity-weighted MNE

$d_{i,j}$ is the SM between the connectivity profile of source i and j

$$J_i \in R_p \rightarrow W(i,j) = \begin{cases} 1 - \frac{1}{d_i} & \text{if } i = j \\ -\frac{d_{i,j}}{\sqrt{d_i d_j}} & \text{if } J_j \in R_p \\ 0 & \text{if } J_j \notin R_p \end{cases}$$

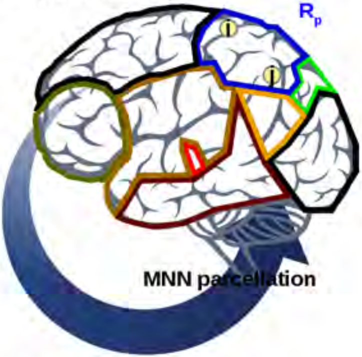

where : $d_i = \sum_{j=1}^{|R_p|} d_{i,j}$

- Total similarity: $d_i = |R_p|$
- Total dissimilarity: $d_i = 1$

- CP estimate is equal to sWMNE when:

$$d_{i,j} = 1 \; \forall i, \forall j$$

[Belaoucha et al 2017]

Similarity-weighted MNE

sWMNE on image viewing dataset [Wakeman et al. 13]

- 11 Subjects.
- T1 image.
- Diffusion weighted images (64 directions).
- EEG (70 electrodes)/MEG (306 sensors)
- fMRI
- 3 classes: photos of familiar, unfamiliar and scrambled faces.

Method comparison

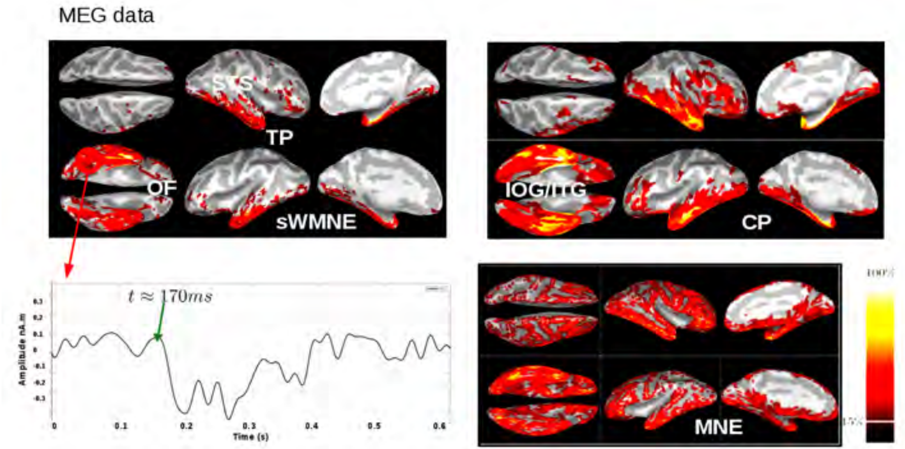

Acknowledgements

Colleagues

Théo Papadopoulo

Alex Gramfort

Rachid Deriche

Jean-Michel Badier

Juliette Leblond

Jan Kybic

Christian Bénar

PhD Students

Anne-Charlotte Philippe

Kostya Maksymenko

Emmanuel Olivi

Sylvain Vallaghé

Christos Papageorgakis

Kai Dang